Journal of Petroleum Science and Engineering 150 (2017) 74–84

Contents lists available at ScienceDirect

Journal of Petroleum Science and Engineering

journal homepage: www.elsevier.com/locate/petrol

Feldspar dissolution with implications for reservoir quality in tight gas sandstones: evidence from the Eocene Es4 interval, Dongying Depression, Bohai Bay Basin, China

Benben Ma[a,b,c,*], Yingchang Cao[b], Yancong Jia[d]

[a] Faculty of Earth Resources, China University of Geosciences, Wuhan 430074, China
[b] School of Geosciences, China University of Petroleum, Qingdao 266580, China
[c] Department of Geosciences, Virginia Tech, Blacksburg, VA 24061, United States
[d] School of Energy Resources, China University of Geosciences, Beijing 100083, China

ARTICLE INFO

Keywords:
Tight gas sandstones
Feldspar dissolution
Dissolution by-products
Reservoir quality
Eocene
Bohai Bay Basin

ABSTRACT

Feldspar dissolution is a pervasive water-rock interaction in siliciclastic sediments and has critical impact on reservoir quality. The purpose of this paper is to evaluate the influence of feldspar dissolution on reservoir quality in tight gas sandstones from the Eocene Es4 interval, Dongying Depression. Based on petrographic, mineralogical, and geochemical analysis, distribution patterns of authigenic minerals associated with feldspar dissolution are recognized. Dissolution of feldspar in Eocene Es4 interval is related to organic acids and CO_2 expelled from adjacent source rocks in deep burial environment. Diffusion is inferred to be the predominant transport mechanism for dissolved solids during feldspar dissolution and result in dissolution by-products (e.g. quartz, kaolinite, illite and albite cements) precipitated in-situ or in adjacent pores. Mass balance calculations also demonstrate most of silica derived from K-feldspar dissolution was precipitated as quartz cements within tight sandstone reservoirs. The net porosities created by feldspar dissolution were insignificant but reservoir permeability was reduced significantly by the precipitation of authigenic quartz, kaolinite, albite, and especially by conversion of kaolinite to hair-like illite at higher temperatures.

1. Introduction

As one of the major unconventional hydrocarbon resources, tight gas sandstone reservoirs are widely distributed in numerous rift basins in China including Bohai Bay, Tarim, Ordos and Sichuan Basins (Zhu et al., 2012; Ren et al., 2014; Lai et al., 2015). In general, tight gas reservoirs are deeply buried and normally characterized by low porosity and permeability (Higgs et al., 2007; Zhu et al., 2012). Moreover, these tight gas reservoirs show strong heterogeneities which are mainly attributed to the significant compaction and cementation (Zou et al., 2012; Lai et al., 2015). In previous studies, secondary porosity, which is defined as the pore space created by dissolution of detrital framework grains and/or authigenic cements, is typically considered as a significant proportion of the total porosity and as the sweet spot for tight gas reservoirs (e.g. Zou et al., 2012; Lai et al., 2015). The enhancement of total porosity during the formation of secondary porosity requires large-scale mass transfer of solids in solution (Bjørlykke, 2014). However, for these tight reservoirs, how does the large scale of mass transfer occur during mineral dissolution to increase the total porosity? Many workers have raised some key controversial issues about the timing of secondary porosity formation related to feldspar dissolution and whether it can enhance total porosity or not during the last 30 years (e.g. Stoessell, 1987; Giles and de Boer, 1990; Bjørlykke and Jahren, 2012). Some geologists have inferred that the majority of secondary porosity probably is created during shallow burial due to leaching by meteoric water (Giles, 1987; Bjørlykke, 2010). This process can make high flux of water available for large scale of mass transport and subsequently, generated an increase in overall porosity for sandstone reservoirs. In contrast, some other workers have ascribed creation of secondary porosity to deep burial environment based on petrographic evidence and geochemical data (e.g. Schmidt and Mcdonald, 1979; Surdam et al., 1989; Rahman and McCann, 2012). As the notable difficulty of transport large amounts of solutes out of sandstone system during deep burial environment, formation of secondary porosity was associated with other mineral reactions that caused precipitation of cements (Chuhan et al., 2001; Bjørlykke and Jahren, 2012). This process probably could not result in net increase in total porosity, but a redistribution of porosity (Giles and

* Corresponding author.
E-mail address: mabenbenupc@163.coms (B. Ma).

http://dx.doi.org/10.1016/j.petrol.2016.11.026
Received 17 January 2016; Received in revised form 12 November 2016; Accepted 18 November 2016
Available online 19 November 2016
0920-4105/

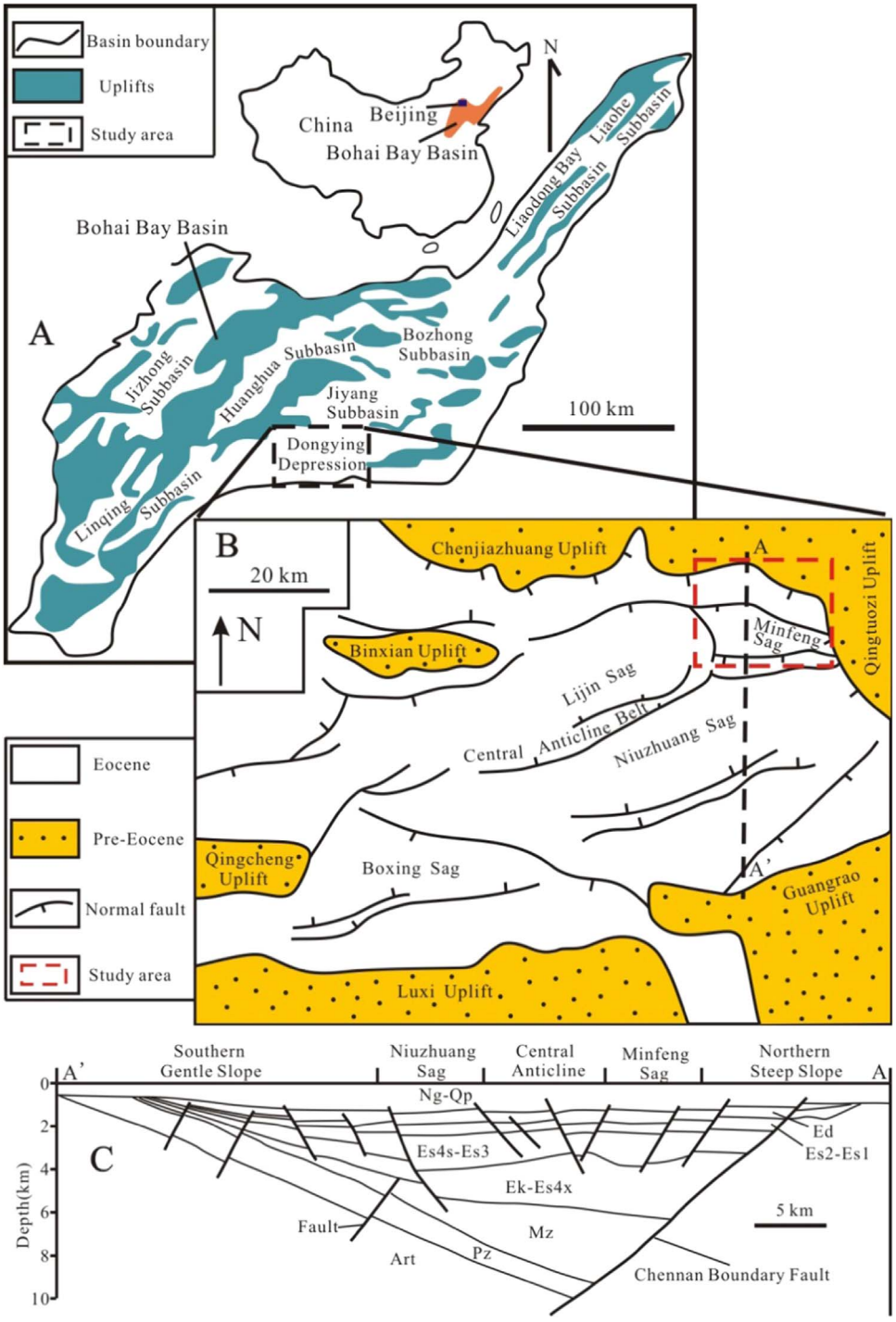

Fig. 1. A. Locality map of subbasins of the Bohai Bay Basin, eastern China (modified from Guo et al., 2010); B. Distribution of main sags and uplifts and major faults and location of section AA'; C. Cross section AA' showing major statigraphic units and major tectonic features within the Dongying Depression (modified from Guo et al., 2010).

de Boer, 1990). Therefore, understanding when the secondary porosity related to feldspar dissolution was formed and whether dissolution by-products were transported out of sandstone reservoirs or not has critical impact on prediction of reservoir quality for tight sandstones.

The Eocene Es4 interval in the Dongying Depression, Bohai Bay Basin in eastern China (Fig. 1) developed in a rift basin and is an important tight gas sandstone interval (Guo et al., 2010; Wang et al., 2014). The Es4 interval consists of sublacustrine-fan, coarse-grained conglomerates, pebbly sandstones, sandstones, and lacustrine mudstones. In addition, the lower unit (Es4x) contains local evaporites in the form of gypsum, anhydrite and halite. With a wide range of burial depths (2500–5000 m), formation temperatures (100–180 °C) and formation pressures (25–70 MPa), the Es4 interval in Dongying Depression is ideally suited to investigate the effects of feldspar dissolution on reservoir quality for tight gas sandstones. Thus, the objectives of this study are to: (1) document the characteristics of feldspar dissolution and other diagenetic minerals using thin section petrography in conjunction with a range of analytical techniques; (2) understand the timing of feldspar dissolution and associated authigenic minerals by utilizing fluid inclusion and burial history analysis; and (3) evaluate the effects of feldspar dissolution on reservoir quality for tight gas sandstones.

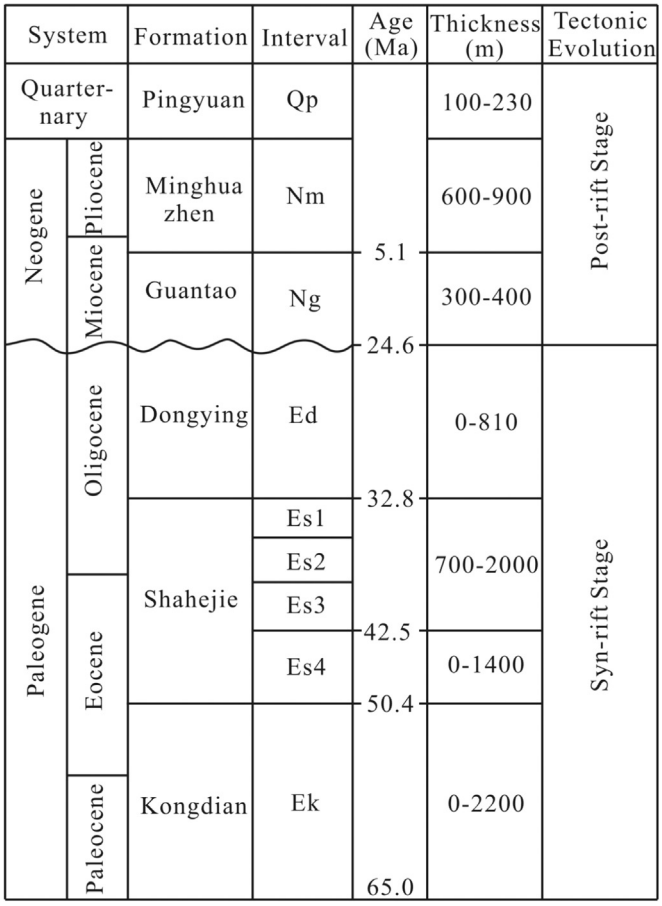

Fig. 2. Tertiary stratigraphy and tectonic evolution of the Dongying Depression.

2. Geological setting

The Dongying Depression covers an area of 5700 km^2 and is located in the southern part of the Jiyang Subbasin of the Bohai Bay Basin (Fig. 1A, B). Tectonic evolution of the depression is subdivided into a syn-rift stage between 65.0 and 24.6 Ma and a post-rift stage from 24.6 Ma to the present (Guo et al., 2010; Dong et al., 2011). Dongying Depression consists of five secondary tectonic provinces from north to south: the northern steep slope, the northern sag (Minfeng Sag), the central anticline, the southern sag (Niuzhang Sag), and the southern gentle slope (Fig. 1C). The Minfeng Sag is located in the northeastern part of the Dongying Depression and the northern margin of the sag is defined by the Chennan Boundary Fault (Fig. 1C; Jiang et al., 2013).

Sedimentary sequences in Dongying Depression, in ascending order, consist of the Paleocene Kongdian (Ek), Shahejie (Es), and Dongying (Ed) formations, the Neogene Guantao (Ng) and Minghuazhen (Nm) formations, and the Quaternary Pingyuan (Qp) Formation (Fig. 2). The Eocene Es4 interval in the Dongying Depression is subdivided by two units (the lower unit Es4x and the upper unit Es4s) and is the subject of this study (Fig. 3; Wan et al., 2010; Wang et al., 2014). The Es4 interval consists of dark lacustrine source rocks, calcareous mudstones interbedded with multi-stage, sublacustrine-fan, sandy conglomerates, pebbly sandstones and sandstones adjacent to the boundary fault (Fig. 3). Evaporites are developed at the bottom and top of Es4x and evaporitic lithologies include gypsum, anhydrite and halite (Fig. 3).

During the initial stage of deposition of Es4x, lake water was saline associated with arid climatic conditions that favored the precipitation of gypsum and subordinate halite (Song et al., 2009; Wang et al., 2014). For most of Es4x deposition, seasonal floods carried abundant siliciclastic sediments into the lake and large-scale of sublacustrine fans developed adjacent to the footwall of the Chennan Boundary Fault and interfingered with more distal mudstones (Fig. 3). A return to arid conditions late in the history of Es4x deposition resulted in a second stage of evaporite precipitation. With a rise in lake level, sublacustrine-fan deposits and interbedded lacustrine mudstones of Es4s developed in the synrift basin. Multi-stage sublacustrine-fan deposits are overall retrogradational and onlap the boundary fault (Fig. 3). This pattern is attributed to long-term rise in lake level (Song et al., 2012).

3. Samples and methods

This study is based on cores from 21 boreholes from the Es4 interval covering depths of 2500–5000 m. A total of 123 thin sections, impregnated with pink epoxy under vacuum and stained with alizarin red-S and potassium ferricyanide (Dickson, 1965), were examined using a standard petrographic microscope. Percentages of framework grains, authigenic cements and porosity were determined by 400 point counts per thin section. The compositions of authigenic minerals and their spatial relationships were investigated in 36 sample chips that were gold-coated using a JSM-5500LV scanning electron microscope (SEM) equipped with a QUANTAX400 energy dispersive X-ray spectra (EDX) under an acceleration voltage of 20 kV using a beam current of 1.0–1.5 nA. In addition, the compositions of albite cements were determined using highly magnified backscatter (BSE) and secondary electron (SE) methods. X-ray diffraction (XRD) analysis using a Ultima IV X-ray diffractometer at the Exploration and Development Research Institute of the Sinopec Zhongyuan Oilfield Company was carried out on <2 μm centrifuged, ethylene glycolated and heated (550 °C) powders to identify clay minerals and their relative abundances.

Seven doubly polished thick sections were prepared for fluid inclusion analysis on quartz overgrowths using a LINKAM THMSG600 heating-freezing stage in the Fluids Research Laboratory in the Department of Geosciences at Virginia Polytechnic Institute and State University. Special attention was paid to identifying fluid inclusion assemblages (FIAs) that represent the most finely discriminated groups of petrographically associated inclusions of fluids that were trapped at the same time (Goldstein and Reynolds, 1994). Homogenization temperature (Th) was measured for fluid inclusions using a heating rate of 10 °C/min at temperatures less than 80 °C and a rate of 5 °C/min at temperatures exceeding 80 °C. This yielded a precision of Th measurements is ± 1 °C.

A total of 175 cylindrical core samples (diameter =25 mm, length =30–40 mm) from 18 boreholes were selected to determine core porosity and permeability at the Exploration and Development Research Institute of the Sinopec Zhongyuan Oilfield Company. The gas expansion method was used for determining porosity and helium was used as the measuring medium. Permeability was measured in a gas-autoclave using the pressure-transient technique (Rahman and McCann, 2012) and nitrogen was used as the permeating medium.

Burial and thermal maturation history curves were plotted using the program BasinMod which adopts the decompaction curve from Falvey and Middleton (1981). Thickness of different lithologies within each formation was obtained from well log data. Ages of each single formation and corresponding paleo-geothermal gradients were collected from several references in the study area (Qiu et al., 2004; Guo et al., 2010). Present temperature and vitrinite reflectance data were also incorporated to correct the present geothermal gradients. In addition, 40 down-well measurements were made of the CO_2 contents of natural gas.

4. Results

4.1. Framework petrology

Most sandstone lithofacies in the Es4 interval are coarse-grained and moderately to poorly sorted lithic arkoses and feldspathic lithar-

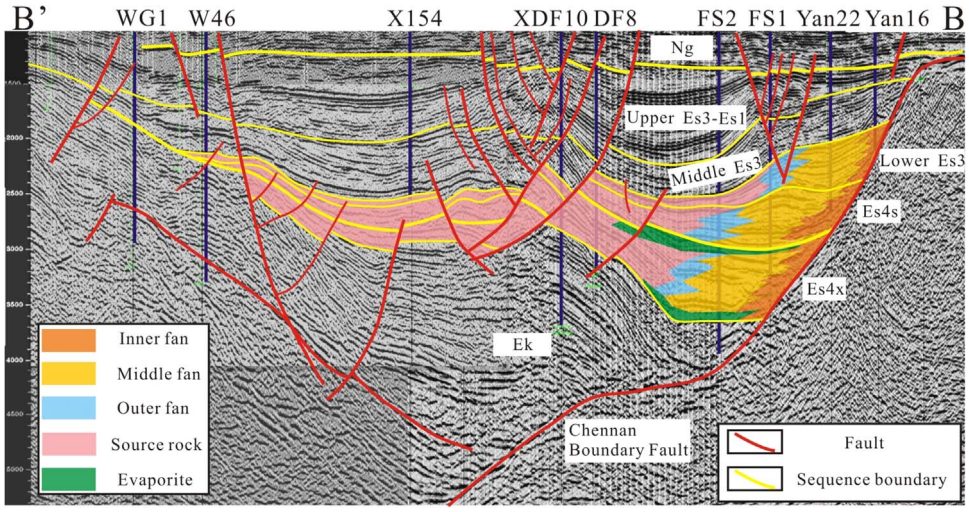

Fig. 3. Interpreted seismic cross section through the study area showing lithologies in the Es4 interval and major extensional faults.

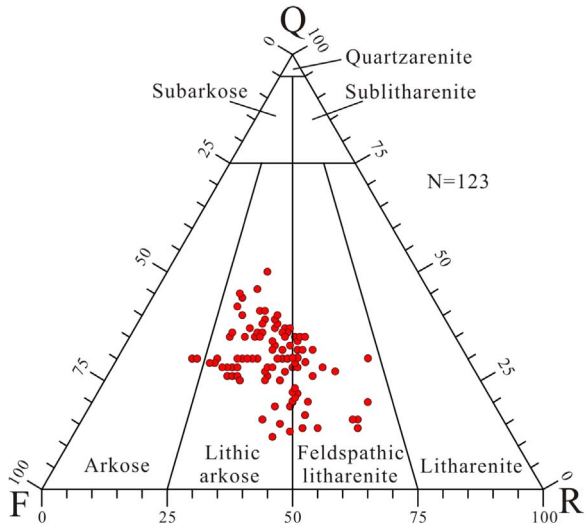

Fig. 4. Compositional ternary plot of point count data following the nomenclature of Folk (1974).

enites (Fig. 4). Framework grain compositions are variable, but feldspar (20–55%, ave. 39%) is the most common framework grain. Rock fragments make up 15–56% (ave. 31%) of the framework grains and include granitic, volcanic, metamorphic and sedimentary grains. Quartz is the least common framework grain (12–50%, ave. 30%).

4.2. Characteristics of feldspar dissolution and associated diagenetic minerals

4.2.1. Feldspar dissolution

Partial to extensive dissolution of detrital feldspar grains was observed in the Es4 interval. Most of the dissolved feldspars are K-feldspar grains (Fig. 5A, B). Locally, dissolved plagioclase can be observed but is not very common. Dissolution of K-feldspar is spatially associated with the formation of authigenic clays (e.g. kaolinite) and quartz cements (Fig. 5A, B, C). Abundances of feldspar dissolution porosity range from 0.1–3.0% with an average of 1.0% and with highest abundances at depths of 2750–3750 m in the Es4 interval (Fig. 6A). Moreover, high contents of feldspar dissolution porosity occur in sandstones at distances of greater than 0.5 m of sandstone-mudstone contacts and decrease abruptly at 3.5 m from the contacts (Fig. 7A).

4.2.2. Quartz cements

Quartz cements commonly occur as syntaxial overgrowths (5–50 μm thick) around detrital quartz grains (Fig. 5D) and, less commonly, as discrete, euhedral, prismatic crystals (5–60 μm in length) within intergranular pores (Fig. 5E). Quartz cements are spatially associated with authigenic kaolinite and illite (Fig. 5D, E). Rarely, two stages of quartz overgrowths can be distinguished based on thin section observation. Abundances of quartz cement range from 0.1–1.5% with an average of 0.5%, with highest abundances at depths of 2750–3750 m in the Es4 interval (Fig. 6B). Moreover, high contents of quartz cement commonly occur in sandstones greater than 0.5 m of sandstone-mudstone contacts and decrease abruptly at 3.5 m from the contacts (Fig. 7B).

4.2.3. Authigenic kaolinite

Authigenic kaolinite occurs as booklets (2–10 μm across) of pseudo-hexagonal crystals (Fig. 5F) that infill primary and secondary pores and replace feldspar framework grains. Well-defined kaolinite patches with similar shapes to feldspar grains fills dissolved pores within feldspar or replace feldspar grains (Fig. 5A, C). Rarely, remnants of feldspar can be observed within kaolinite patches. The proportion of kaolinite cements as a percentage of all clay minerals present decreases with depth and shows a rapid decline at a depth of approximately 3250 m (Fig. 8A).

4.2.4. Authigenic illite

Authigenic illite commonly displays hair-like crystals and fibrous aggregates (Fig. 5D, E). It mainly occurs as pore-filling cements and as replacement of potassium feldspar (Fig. 5B). Authigenic illite normally replaces or engulfs authigenic kaolinite (Fig. 5F). The proportion of illite cement increases with depth and shows a rapid increase at a depth of about 3250 m (Fig. 8B).

4.2.5. Albite cements

Authigenic feldspar cements are predominantly in the form of albite (trace to 2.5%). Euhedral albite crystals are present as pore-filling cements and as replacement of dissolved plagioclase and K-feldspar (Fig. 5G, H). Authigenic albite typically grows along twining and cleavage planes of detrital feldspar grains (Fig. 5H). In rare cases, euhedral albite crystals are coated by authigenic illite (Fig. 5I). Albitization of K-feldspar and plagioclase are most common, especially in Es4x, at greater burial depths.

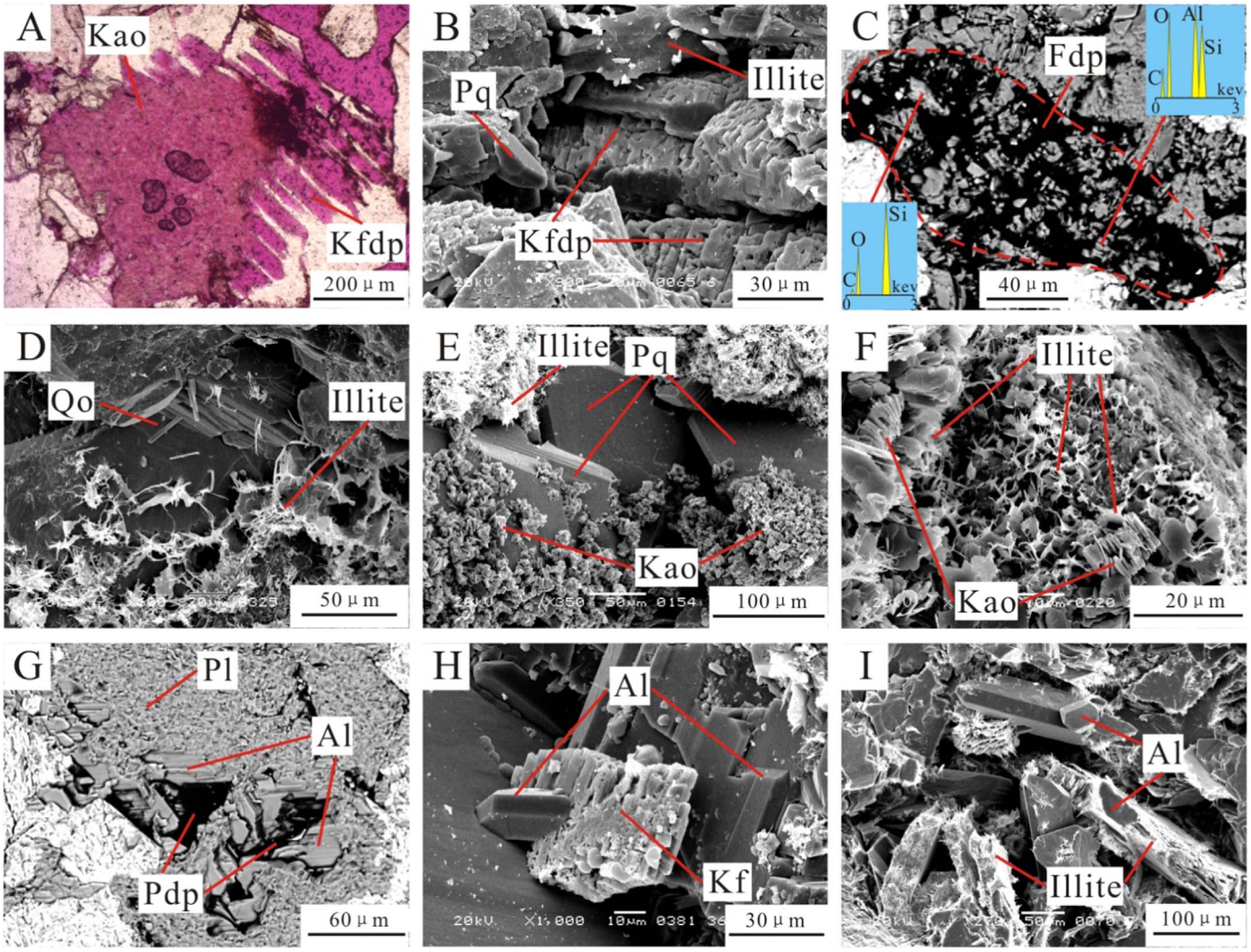

Fig. 5. Photomicrographs of feldspar dissolution, authigenic kaolinite, illite, quartz and albite cements in the Es4 interval. A. Secondary porosity related to feldspar dissolution along cleavage planes and authigenic kaolinite precipitation in adjacent pores, Well YX21, 3137.7 m; B. SEM image of secondary porosity related to K-feldspar dissolution along cleavage planes and associated with precipitation of prismatic quartz and illite cements, Well FS10, 4323.7 m; C. BSE image of authigenic quartz and kaolinite filling in feldspar dissolution pores, Well Yong92, 2968.77 m; D. SEM image of quartz overgrowth enclosed by authigenic illite, Well Yong 928, 3844.75 m; E. SEM image of prismatic quartz surrounded by authigenic kaolinite and illite, Well Y22, 3239.1 m; F. SEM image of blocky aggregates of pseudo-hexagonal plates of kaolinite replaced by illite, Well Y22-X1, 3367 m; G. BSE image of euhedral albite crystals replacing dissolved plagioclase, Well Yong92, 2968.77 m; H. SEM image of euhedral albite crystals as pore-filling cements enclosing K-feldspar grain and partially replacing a detrital feldspar grain (Primarily K-feldspar), Well Y222, 4014.66 m; I. SEM image of euhedral albite crystals as pore-filling cements and coated by authigenic illite, Well FS10, 4326 m. Kao=kaolinite, Kfdp=K-feldspar dissolution pores, Pq=Prismatic quartz, Fdp=Feldspar dissolution pores, Qo=Quartz overgrowths, Pl=Plagioclase, Pdp=Plagioclase dissolution pores,Al =Albite, Kf=K-feldspar.

4.3. Mineral chemistry

4.3.1. Compositions of albite cements

BSE image and SEM-EDX point analyses confirm the presence of albite cements. In total, 29 points of partially or totally albitized feldspar were analyzed. Elemental weight percentages (%) of Na^{+}, Ca^{2+} and K^{+} were used to calculate moles and were normalized to molecular percentages. These percentages were plotted on a ternary diagram with anorthite, albite and K-feldspar end members (Fig. 9). The data show that 19 of the 29 analyses are pure albite (Table 1).

4.3.2. Fluid inclusions

Fluid inclusion assemblages (FIAs) in quartz overgrowths typically occur along the boundaries with the detrital grains (Fig. 10A, B). Most of FIAs contain measurable, two-phase fluid inclusions ≥5 μm in size. Homogenization temperatures (Th) were obtained from 48 aqueous inclusions. In addition, most FIAs are characterized by consistent Th values (temperature difference commonly less than 15 °C) and indicate these FIAs probably have not been altered by thermal reequilibration after their entrapment (e.g. Goldstein, 2001). The two different generations of quartz overgrowths produced resolvable populations of Th (Fig. 10C; Table 2). Th values of the first-generation inclusions range from 98 to 129 °C with a peak at 110–120 °C whereas the second-generation inclusions ranges from 136 to 186 °C with a peak at 160–170 °C (Fig. 10C).

4.4. Porosity and permeability

Porosity and permeability data determined for 175 core samples reveal that, in general, the reservoir properties for Eocene Es4 interval are relatively poor. The core porosity varies from 0.4–17.6% with an average of 6.7%, whereas the core permeability ranges from 0.001 to 29.51 mD with an average of 0.94 mD (Fig. 11). Therefore, the Eocene Es4 sandstones pertain to typical tight gas reservoirs with extremely low porosity and permeability. The reservoirs also show wide variations in porosity and permeability as well as weak correlation between porosity and permeability (Fig. 11).

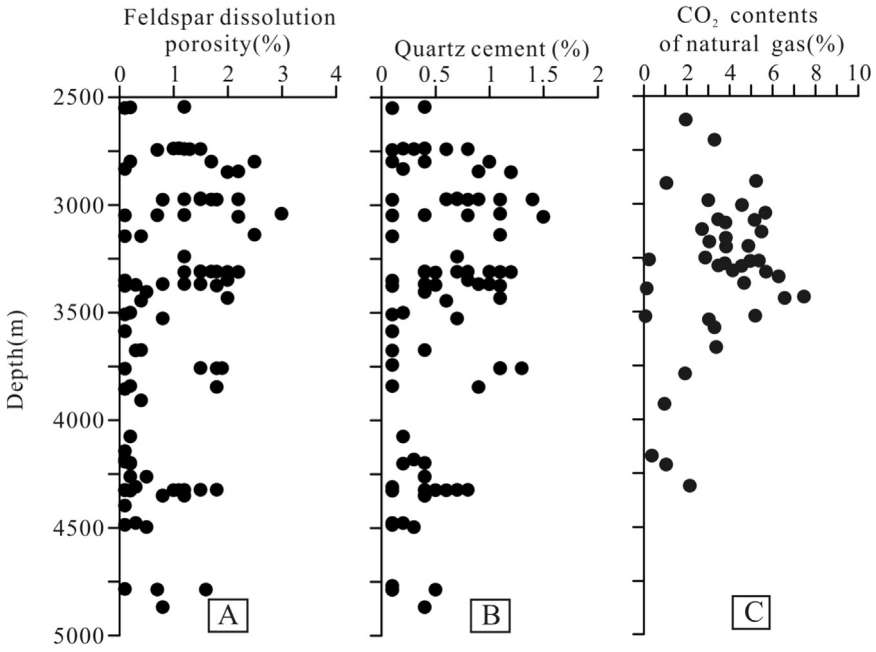

Fig. 6. A. Plot showing the variation in the percentages of feldspar dissolution porosity with depth; B. Plot showing the variation in the percentages of quartz cement with depth. Based on point counting of 123 thin sections from 21 boreholes in the Es4 interval; C. Plot showing the variation in CO_2 contents of natural gas with depth (40 data points from 11 Boreholes in Es4 interval).

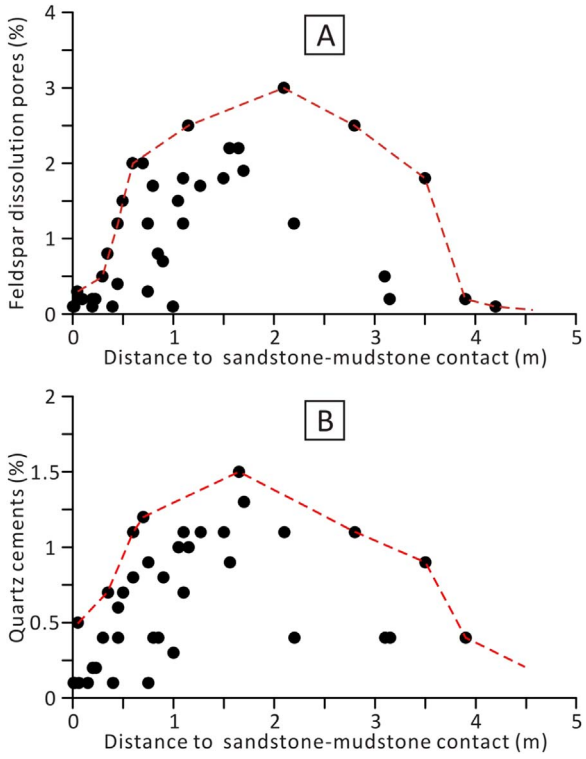

Fig. 7. A. Cross-plot of contents of feldspar dissolution porosity versus distance to sandstone-mudstone contact; B. Cross-plot of contents of quartz cements versus distance to sandstone-mudstone contact.

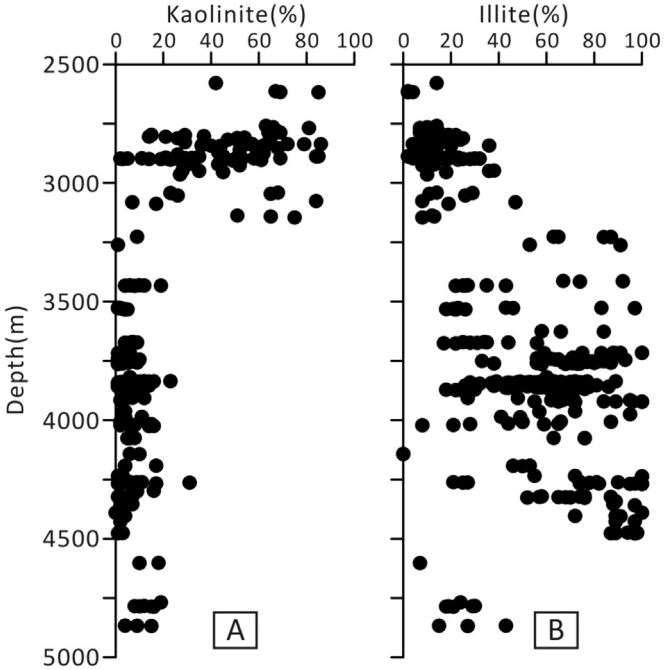

Fig. 8. Plots showing variations in percentages of authigenic kaolinite and illite in sandstones as a function of depth.

5. Discussion

5.1. Burial and thermal history

Following deposition, the Eocene Es4 succession experienced rapid and continuous subsidence (Fig. 12) except for a major uplift event that occurred prior to deposition of the Guantao Formation. Although this major uplift event resulted in erosion and development of a regional unconformity, the Es4 interval was not exposed but was overlain by up to 1,800 m of lacustrine and fluvial sediments. Based on Ro values, most of Es4s is within the liquid hydrocarbon window corresponding to reflectance values of 0.5–1.3%. In contrast, the lower parts of Es4x are within the gas generation window corresponding with reflectance values of 1.3–2.0% (East et al., 2012).

5.2. The origin of feldspar dissolution

The presence of evaporite beds and black mudstones in the Eocene

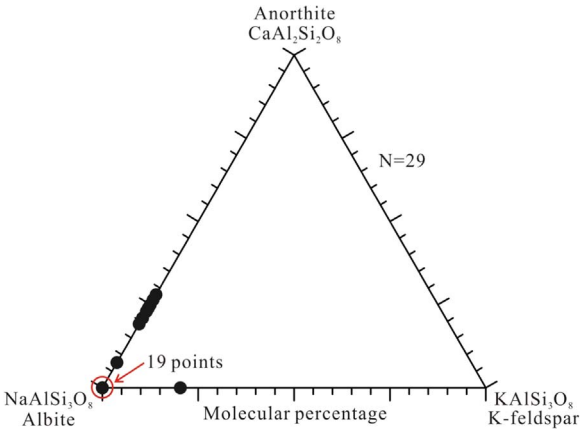

Fig. 9. Chemical compositions of albite cements in the Es4 interval (29 data points from 3 boreholes in the Es4 interval of which 19 data points are pure albite).

Table 1
EDX analyses of albite cements in the Es4 interval.

Well	Depth (m)	Strata	Molecular (%)		
			$CaAl_2Si_2O_8$	$NaAlSi_3O_8$	$KAlSi_3O_8$
Y22–22	3508.1	Es4s	20.97	79.03	bdl
Yong92	2968.77	Es4s	23.91	76.09	bdl
Yong92	2968.77	Es4s	24.90	75.10	bdl
Yong92	2968.77	Es4s	19.18	80.82	bdl
Yong92	2968.77	Es4s	22.95	77.05	bdl
Yong92	2968.77	Es4s	bdl	100.00	bdl
Yong92	2968.77	Es4s	bdl	100.00	bdl
Yong92	2968.77	Es4s	bdl	100.00	bdl
Yong92	2968.77	Es4s	bdl	100.00	bdl
Yong92	2968.77	Es4s	bdl	100.00	bdl
Yong92	2968.77	Es4s	bdl	100.00	bdl
Yong92	2968.77	Es4s	bdl	100.00	bdl
Yong92	2968.77	Es4s	7.59	92.41	bdl
Yong92	2968.77	Es4s	bdl	100.00	bdl
Yong92	2968.77	Es4s	bdl	100.00	bdl
Yong92	2968.77	Es4s	bdl	100.00	bdl
Yong92	2968.77	Es4s	bdl	100.00	bdl
Yong92	2968.77	Es4s	bdl	100.00	bdl
Yong92	2968.77	Es4s	bdl	100.00	bdl
Yong92	2968.77	Es4s	bdl	100.00	bdl
Yong92	2968.77	Es4s	26.44	73.56	bdl
Yong92	2968.77	Es4s	28.00	72.00	bdl
Yong92	2968.77	Es4s	bdl	100.00	bdl
Yong92	2968.77	Es4s	20.94	79.06	bdl
Yong92	2968.77	Es4s	bdl	100.00	bdl
Yong92	2968.77	Es4s	bdl	79.67	20.33
Y22	3239.1	Es4s	bdl	100.00	bdl
Y22	3239.1	Es4s	bdl	100.00	bdl
Y22	3239.1	Es4s	bdl	100.00	bdl

bdl=below detect limit.

Es4 interval has been used to suggest that early burial fluids were reducing and saline with little influence of meteoric water (Xu et al., 2008). With rapid subsidence and quick depositional rates (Fig. 12), the majority of lacustrine sediments has extremely short residence time to exposure to meteoric water environment but is characterized by relatively long residence time in reduced depositional environment. Evidence for anoxic and reduced environment during Es4 deposition is provided by the black color of mudstones and the dark grey to grey color of conglomerates, pebbly sandstones and sandstones (Ma et al., 2016). Red beds are notably lacking. As discussed above, although a major uplift event occurred, the Eocene Es4 interval was still overlain by thick lacustrine and fluvial sediments. Therefore, meteoric waters had little impact on deep sublacustrine reservoirs in the Es4 interval.

In the deep burial environment, the dissolution of feldspar is attributed to organic acids and CO_2 derived from thermal maturation of organic matter in adjacent source rocks as proposed by Surdam et al. (1989) and Morad et al. (2000). Highest concentrations of organic acid in pore fluids occur in the temperature range of 80–120 °C (Surdam et al., 1989) resulting in extensive dissolution of the aluminosilicates. Moreover, maximum concentrations of CO_2 in natural gas occur at depths of 2750–3750 m (Fig. 6C) that correspond with the highest abundances of feldspar dissolution porosity (Fig. 6A). Therefore, it is inferred that organic acids and CO_2 derived from adjacent source rocks contribute to feldspar dissolution within sandstones.

5.3. Characteristics of dissolution by-products

Feldspar is extensively dissolved in the Es4 interval and is spatially associated with inferred by-products such as authigenic quartz and clays (Fig. 5A, B, C). Dissolution of feldspar (e.g. K-feldspar) can be expressed by Eq. (1):

$$2KAiSi_3O_8 + 2\quad H^+ + H_2O = Al_2Si_2O_5(OH)_4 + 2\quad K^+ + 4SiO_2 \qquad (1)$$

where $KAiSi_3O_8$ is K-feldspar, $Al_2Si_2O_5(OH)_4$ is kaolinite, and SiO_2 is quartz.

Quartz cements are sparsely developed in the Es4 interval (Fig. 6B) and occur as two populations of quartz overgrowths: the first at temperatures of 110–120 °C and the second at160–170 °C (Fig. 10C). Potential important sources of quartz cements in these systems include clay transformations in adjacent mudstones (Peltonen et al., 2009), pressure solution of detrital grains (Harwood et al., 2013) and feldspar dissolution (Worden and Morad, 2000). Within the Es4 interval, feldspar dissolution is common and the scarcity of concavo-convex or sutured contacts probably indicates that pressure solution was not an important source of quartz cements. As the low concentrations of silica in pore fluids (typically < 65 ppm at 100 °C; Bjørlykke and Jahren, 2012), it is not possible to transport silica over long distances from external sources (Thyne, 2001; Bjørlykke and Jahren, 2012). Quartz cements do not show an increasing trend with depth and have highest abundances at depths of 2750–3750 m (Fig. 6B) corresponding with zones of extensive feldspar dissolution. Moreover, well correlation between the contents of feldspar dissolution porosity and quartz cements (Fig. 13), indicate one volume of dissolved feldspar could approximately generate 0.48 vol of quartz cement. Mass balance calculations demonstrate, one volume of dissolved K-feldspar grains produces 0.42 volumes of silica to forming quartz cement. Therefore, most (if not all) of silica derived from K-feldspar dissolution was precipitated in-situ or in adjacent pores (thin section scale) as quartz cements within sandstones. The temperature range (80–120 °C) also is consistent with the homogenization temperatures of first-generation quartz overgrowths (110–120 °C) suggesting that authigenic quartz in the Es4 interval was derived from dissolution of feldspar. Probable sources for the late-stage quartz cements are feldspar dissolution by organic CO_2 derived from decarboxylation of organic acids at high temperatures (120–160 °C) (e.g. Surdam et al., 1989).

Authigenic kaolinite filling dissolved pores within feldspar (Fig. 5A, C) and spatially associated with quartz cements (Fig. 5F) probably indicate it is formed synchronously with feldspar dissolution. Formation of kaolinite cement is dependent on availability of Al^{3+} in pore fluids (Stoessell, 1987; Hayes and Boles, 1992). Solubility of aluminum is extremely low, in general, and the content of aluminum in formation waters is typically less than 1 ppm (Bjørlykke and Jahren, 2012). However, Al^{3+} derived from dissolved feldspar can complex with carboxylic acids and result in an increase in aluminum solubility (Surdam et al., 1989). Resulting kaolinite is precipitated in-situ or in adjacent pores in the Es4 interval. Illitization of kaolinite probably occurred as evidenced by authigenic kaolinite replaced by authigenic illite (Fig. 5F). Moreover, variation in proportions of authigenic kaolinite and illite is a function of present burial depth (Fig. 8A, B) and indicate that kaolinite was converted to illite with increasing

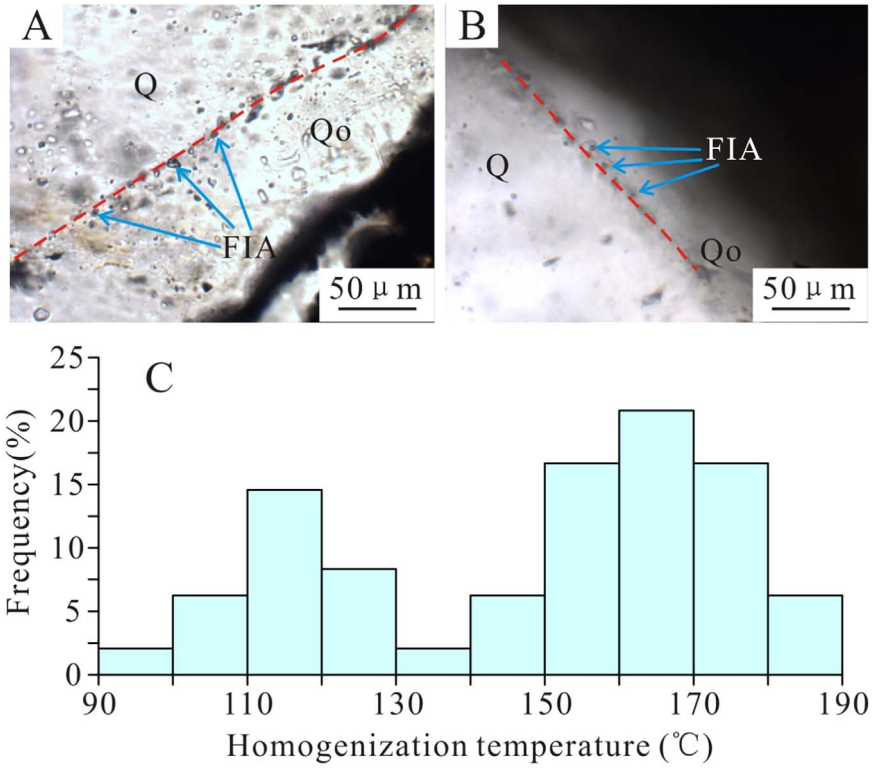

Fig. 10. A-B. Photomicrographs of aqueous inclusions in quartz overgrowths; C. Histograms of homogenization temperatures of aqueous inclusions in quartz overgrowths in the Es4 interval (48 data points from 7 boreholes). Q = Quartz grain, Qo = Quartz overgrowths, FIA = Fluid inclusion assemblage.

Table 2
Microthermometric data of aqueous fluid inclusions for quartz overgrowths in the Es4 interval.

Well	Depth (m)	Strata	Th (°C)	FIA	Well	Depth (m)	Strata	Th (°C)	FIA
Yong92	2971.92	Es4s	116	1	Yong928	3844.75	Es4s	147	1
Yong92	2971.92	Es4s	126	1	F8	4199.51	Es4x	122	1
Yong92	2971.92	Es4s	123	1	F8	4199.51	Es4x	129	1
Yong92	2971.92	Es4s	153	2	F8	4199.51	Es4x	161	2
Yong92	2971.92	Es4s	161	2	F8	4199.51	Es4x	166	2
Yong92	2971.92	Es4s	136	2	F8	4199.51	Es4x	168	2
YX21	3137.7	Es4s	115	1	FS3	4867	Es4x	170	1
YX21	3137.7	Es4s	113	1	FS3	4867	Es4x	174	1
YX21	3137.7	Es4s	116	1	FS3	4867	Es4x	165	1
YX21	3137.7	Es4s	112	2	FS3	4867	Es4x	172	2
YX21	3137.7	Es4s	114	2	FS3	4867	Es4x	186	2
YX21	3137.7	Es4s	100	2	FS3	4867	Es4x	178	2
YX21	3137.7	Es4s	153	3	FS3	4867	Es4x	176	2
YX21	3137.7	Es4s	157	3	FS3	4867	Es4x	146	3
Y22	3239.1	Es4s	98	1	FS3	4867	Es4x	153	3
Y22	3239.1	Es4s	101	1	FS3	4867	Es4x	158	3
Y22	3239.1	Es4s	110	1	FS3	4867	Es4x	152	3
Y22	3239.1	Es4s	105	1	FS3	4867	Es4x	161	4
Y22–22	3444.4	Es4s	153	1	FS3	4867	Es4x	168	4
Y22–22	3444.4	Es4s	160	1	FS3	4867	Es4x	162	4
Y22–22	3444.4	Es4s	149	1	FS3	4867	Es4x	166	4
Yong928	3844.75	Es4s	178	1	FS3	4867	Es4x	173	5
Yong928	3844.75	Es4s	184	1	FS3	4867	Es4x	180	5
Yong928	3844.75	Es4s	175	1	FS3	4867	Es4x	181	5

burial. At greater depth (> 130 °C, e.g. Morad et al., 2000; Bjørlykke and Jahren, 2012), the presence of K-feldspar will increase the ratio of K^+: H^+ and move the pore water from the stability of kaolinite to that of illite (Fig. 14). Illitization of kaolinite can be expressed by Eq. (2):

$$KAiSi_3O_8 + Al_2Si_2O_5(OH)_4 = KAl_3Si_3O_{10}(OH)_2 + 2SiO_2 + H_2O \quad (2)$$

where $KAl_3Si_3O_{10}(OH)_2$ is illite.

Replacement of dissolved plagioclase and K-feldspar grains by authigenic albite (Fig. 5G, H) demonstrates authigenic albite is another by-product of feldspar dissolution. At low temperature, kaolinite would be more stable. With increasing temperature, the acidity of pore fluids decreases and the ratio of Na^+: H^+ increases. As a result, the stability field of kaolinite is much reduced (Fig. 14) and could react with silica to form albite as expressed by Eq. (3):

$$Al_2Si_2O_5(OH)_4 + 2Na^+ + 4SiO_2 = NaAiSi_3O_8 + 2 \quad H^+ + H_2O \quad (3)$$

where $NaAiSi_3O_8$ is albite. Combining Eq. (1) with Eq. (3), the resulting Eq. (4) can be expressed as below:

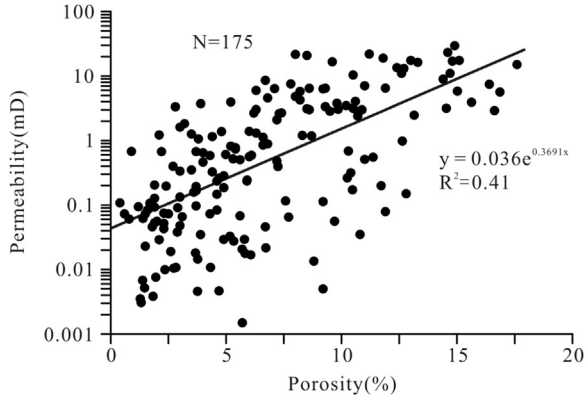

Fig. 11. Cross-plot of core porosity and permeability for Eocene Es4 sandstones.

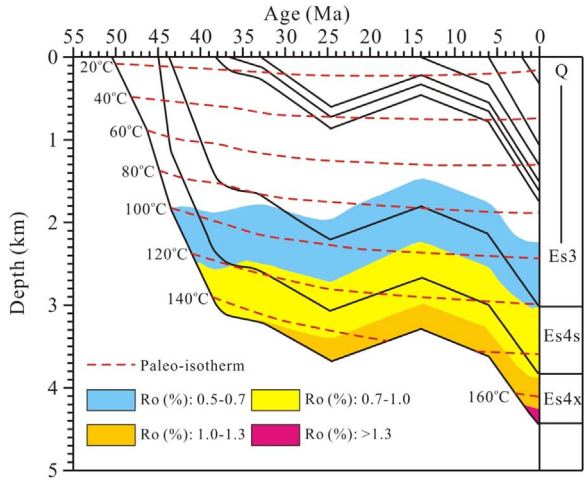

Fig. 12. Burial history plot for Well FS1 showing isotherms and vitrinite reflectance (Ro) data.

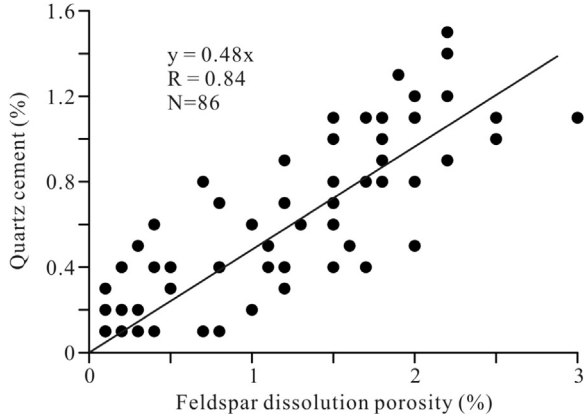

Fig. 13. Cross-plot of feldspar dissolution porosity versus quartz cement.

$$KAiSi_3O_8 + Na^+ = NaAiSi_3O_8 + K^+ \quad (4)$$

It is demonstrated that, as K-feldspar (or plagioclase) was dissolved progressively, K^+(or Ca^{2+}) ions could be substituted by Na^+ ions and this process resulted in precipitation of pure albite (Fig. 9). In addition, the source of sodium probably is derived from dissolution of plagioclase grains which consist of certain percentage of albite (e.g. Mansurbeg et al., 2008). Pore-waters also are a significant source of sodium for albitization particularly where associated with evaporites (e.g. halite) such as in Es4x.

In general, at the initial stage of feldspar dissolution, dissolution by-products are authigenic quartz and kaolinite (Fig. 5C). With increasing temperature, the acidity of pore fluids decreases and the ratio of K^+:H^+ and Na^+:H^+ increases respectively. Therefore, the early-formed dissolution by-products will be transformed to authigenic illite and albite. They are more stable and can coexist at higher temperature (Fig. 5I).

5.4. Transport mechanism for feldspar dissolution

The reaction rate between the crystal and the pore fluids is of critical impact on the mass transport process (e.g. Aagaard and Helgeson, 1982; Giles, 1987). In the deep burial environment, the reaction rate of feldspar dissolution is greater than the rate of transport away from the crystal surface. With increasing temperature, the increase in reaction rates will make the dissolved solids more concentrated around the crystals and set up steep concentration gradients between the crystals and pore fluids (Fig. 15). Consequently, the dissolved solids are typically driven by diffusion and result in dissolution by-products (e.g. authigenic quartz and kaolinite) precipitated in-situ or in adjacent pores. Diffusion is considered to have been the predominant transport mechanism for dissolved solids over short distances (e.g. thin-section scale) at low flow velocity as noted by other authors (e.g. Giles, 1987; Bjørlykke, 1998; Ahmed, 2002). Moreover, the close spatial association between feldspar dissolution and authigenic quartz cementation well removed from sandstone-mudstone contacts (Fig. 7A, B) demonstrates that dissolved silica was transported very short distances (several centimeters) and this process is consistent with slow diffusive transport (e.g. Mullis, 1992).

5.5. Impact of feldspar dissolution on reservoir quality

Formation of secondary porosity related to feldspar dissolution is widely considered to enhance reservoir quality (e.g. Mansurbeg et al., 2008; Rahman and McCann, 2012) but, in the Eocene Es4 interval, the by-products of feldspar dissolution (e.g. authigenic quartz, kaolinite, illite and albite cements) precipitated in-situ or in adjacent pores. As discussed above, feldspar dissolution in the Eocene Es4 interval occurred in the deep burial environment. Large-scale of mass transfer probably could not occur due to strong heterogeneities in the deeply buried tight sandstones. Moreover, based on mass balance calculations, silica derived from K-feldspar dissolution could mostly re-precipitated as quartz cements within sandstone reservoirs. Therefore, the net porosities created by feldspar dissolution were insignificant.

The correlation between core porosity and core permeability of sandstones with different percentages of feldspar dissolution porosity can be adopted to estimate the influence of feldspar dissolution on reservoir permeability (Giles and de Boer, 1990). The long-axis slope for these three ellipses increases ($K_1 > K_2 > K_3$) as feldspar dissolution porosity decreases (Fig. 16). Sandstone samples with the same core porosity but more percentage of feldspar dissolution porosity favor to have lower permeability (Fig. 16). The reason for this phenomenon is that, with increasing burial, pore types were changed from primary macropores to secondary pores and micropores by the precipitation of authigenic quartz, kaolinite, albite, and especially by conversion of kaolinite to hair-like illite at higher temperatures. The sum result of these processes was the reduction of reservoir permeability.

6. Conclusions

Feldspar dissolution has a critical impact on reservoir quality as exemplified by tight gas sandstone reservoirs in the Eocene Es4 interval in the Dongying Depression, Bohai Bay Basin, China. This study has demonstrated that:

(1) The Eocene Es4 sandstones in the Dongying Depression pertain to typical tight gas reservoirs with a range of porosity from 0.4–17.6% (ave. 6.7%) and permeability from 0.001 to 29.51 mD (ave. 0.94 mD).

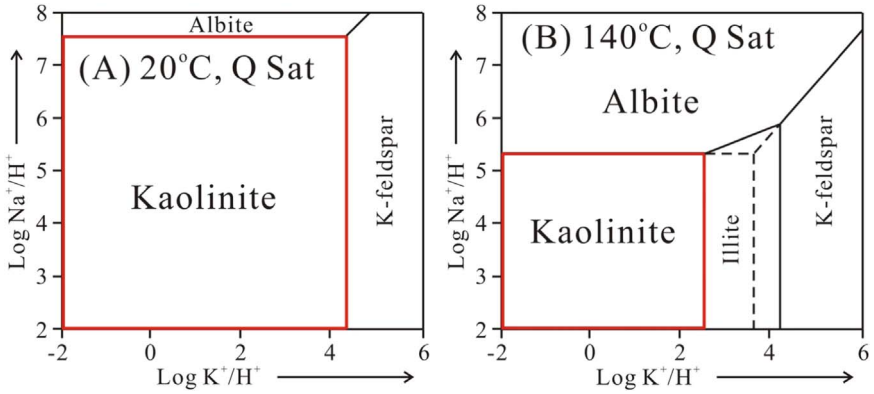

Fig. 14. Activity diagram showing the stability fields of kaolinite are reduced with increasing temperature (modified from Bjørlykke, 2014). Q Sat refers to quartz saturation.

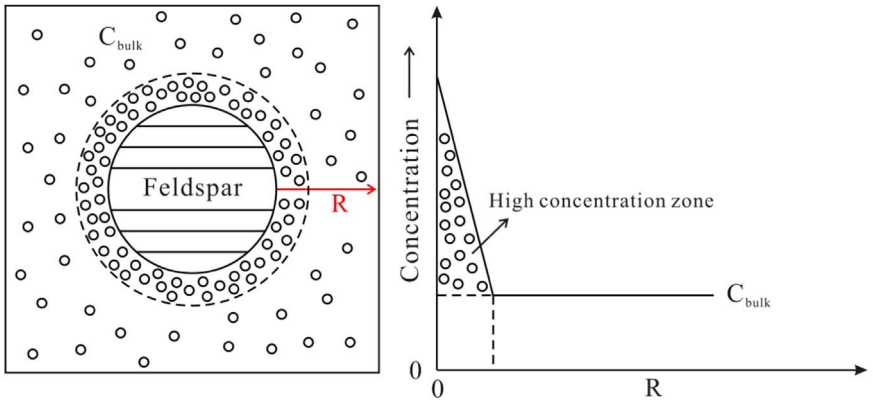

Fig. 15. Transport mechanism for feldspar dissolution reaction (adapted from Giles, 1987). R refers to radial distance from crystal surface; C_{bulk} refers to concentration in the bulk pore fluid.

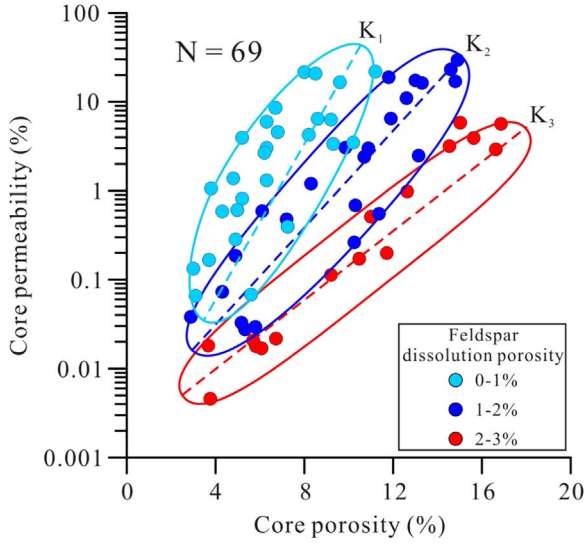

Fig. 16. Cross-plot of core porosity and permeability with different percentages of feldspar dissolution porosity.

(2) Feldspar dissolution in the Eocene Es4 interval in Dongying Depression is mainly attributed to organic acids and CO_2 derived from adjacent source rocks in deep burial environment. Feldspar dissolution is spatially associated with dissolution by-products. At the initial stage of feldspar dissolution, dissolution by-products are authigenic quartz and kaolinite. With increasing temperature, the early-formed dissolution by-products will be transformed to authigenic illite and albite.

(3) The main transport mechanism for feldspar dissolution is predominated by diffusion and result in dissolution by-products precipitated in-situ or in adjacent pores. Mass balance calculations demonstrate most of silica derived from K-feldspar dissolution was precipitated as quartz cements within sandstone reservoirs.

(4) Formation of secondary porosity related to feldspar dissolution is spatially with the by-products (e.g. authigenic quartz, kaolinite, illite and albite cements) precipitated in-situ or in adjacent pores. The net porosities created by feldspar dissolution were insignificant. Reservoir permeability was reduced significantly by precipitation of dissolution by-products, especially by conversion of kaolinite to hair-like illite at higher temperatures.

Acknowledgments

This research was financially supported by the National Natural Science Foundation of China (41102058), Key Program for National Natural Science Foundation of China (U1262203), National Oil & Gas Major Project of China (2011ZX05006-003), and an Excellent Doctoral Dissertation award supported by China University of Petroleum (LW140101A). Benben Ma thanks the China Scholarship Council (CSC) for supporting his one year research stay in the U.S.A.

References

Aagaard, P., Helgeson, P.C., 1982. Thermodynamic and kinetic constraints on reaction rates among minerals and aqueous solutions. I. Theoretical considerations. Am. J. Sci. 282, 237–285.

Ahmed, W., 2002. Diagenesis and mass transfer between Permo-Triassic sandstones and interbedded mudstones, Ulster Basin. Bull. Chem. Soc. Ethiop. 16, 9–35.

Bjørlykke, K., 1998. Clay mineral diagenesis in sedimentary basins a key to the prediction of rock properties: examples from the North Sea Basin. Clay Miner. 33, 15–34.

Bjørlykke, K., 2010. Petroleum geoscience: from sedimentary environments to rock physics. Springer Verlag, New York, 507.

Bjørlykke, K., 2014. Relationships between depositional environments, burial history and

rock properties. Some principal aspects of diagenetic process in sedimentary basins. Sediment. Geol. 301, 1–14.
Bjørlykke, K., Jahren, J., 2012. Open or closed geochemical systems during diagenesis in sedimentary basins: constraints on mass transfer during diagenesis and the prediction of porosity in sandstone and carbonate reservoirs. AAPG Bull. 96, 2193–2214.
Chuhan, F., Bjørlykke, K., Lowrey, C.J., 2001. Closed-system burial diagenesis in reservoir sandstones: example from the Garn Formation at Haltenbanken area, offshore Mid-Norway. J. Sediment. Res. 71, 15–26.
Dickson, J.A., 1965. Carbonate identification and genesis as revealed by staining. J. Sediment. Pet. 27, 107–118.
Dong, W., Lin, C.S., Eriksson, K.A., Zhou, X.H., Liu, J.Y., Teng, Y.B., 2011. Depositional systems and sequence architecture of the Oligocene Dongying Formation, Liaozhong Depression, Bohai Bay Basin, northeast China. AAPG Bull. 95, 1475–1493.
East, J.A., Swezey, C.S., Repetski, J.E., Hayba, D.O., 2012. Thermal maturity map of Devonian shale in the Illinois, Michigan, and Appalachian basins of North America. USA. Geological Survey Scientific Investigations Map. 1 sheet 3214.
Falvey, D.A., Middleton, M.F., 1981. Passive continental margins: evidence for a pre-breakup deep crustal metamorphic subsidence mechanism. 26th International Geophysical Congress, Colloquia C3.3. Geol. Cont. Margins. Oceanol. Acta 4, 103–114.
Folk, R.L., 1974. Petrology of Sedimentary Rocks. Hemphill Press, Texas, 182.
Giles, M.R., 1987. Mass transfer and problems of secondary porosity creation in deeply buried hydrocarbon reservoirs. Marine Pet. Geol. 4, 188–204.
Giles, M.R., de Boer, R.B., 1990. Origin and significance of redistributional secondary porosity. Marine Pet. Geol. 7, 378–396.
Goldstein, R.H., 2001. Fluid inclusions in sedimentary and diagenetic systems. Lithos 55, 159–193.
Goldstein, R.H., Reynolds, T.J., 1994. Systematics of fluid inclusions in diagenetic minerals. SEPM Short Course 31, 199.
Guo, X.W., He, S., Liu, K.Y., Song, G.Q., Wang, X.J., Shi, Z.S., 2010. Oil generation as the dominant overpressure mechanism in the Cenozoic Dongying Depression, Bohai Bay Basin, China. AAPG Bull. 94, 1859–1881.
Harwood, J., Aplin, A.C., Fialips, C.I., Iliffe, J.E., Kozdon, R., Ushikubo, T., Valley, J.W., 2013. Quartz cementation history of sandstones revealed by high-resolution SIMS oxygen isotope analysis. J. Sediment. Res. 83, 522–530.
Hayes, M.J., Boles, J.R., 1992. Volumetric relationships between dissolved plagioclase and kaolinite in sandstones: implications for aluminum mass transfer in the San Joaquin Basin, California. In: Origin, Diagenesis, and Petrophysics of Clay Minerals in Sandstones 47. SEPM Special Publication, Tslua, Okla., United States, 111–123.
Higgs, K.E., Zwingmann, H., Reyes, A.G., Funnell, R.H., 2007. Diagenesis, porosity evolution, and petroleum emplacement in tight gas reservoirs, Taranaki basin, New Zealand. J. Sediment. Res. 77, 1003–1025.
Jiang, S., Henriksen, S., Wang, H., Lu, Y.C., Ren, J.Y., Cai, D.S., Feng, Y.L., Weimer, P., 2013. Sequence-stratigraphic architectures and sand-body distribution in Cenozoic rifted lacustrine basins, east China. AAPG Bull. 97, 1447–1475.
Lai, J., Wang, G., Ran, Y., Zhou, Z., 2015. Predictive distribution of high-quality reservoirs of tight gas sandstones by linking diagenesis to depositional facies: Evidence from Xu-2 sandstones in the Penglai area of the central Sichuan basin China. J. Nat. Gas Sci. Eng. 23, 97–111.
Ma, B., Cao, Y., Eriksson, K., Jia, Y., Wang, Y., 2016. Burial evolution of evaporites with implications for sublacustrine fan reservoir quality: a case study from the Eocene Es4x interval, Dongying Depression, Bohai Bay Basin, China. Marine Pet. Geol. 76, 98–114.
Mansurbeg, H., Morad, S., Salem, A., Marfil, R., El-ghali, M.A.K., Nystuen, J.P., Caja, M.A., Amorosi, A., Garcia, D., Iglesia, A.L., 2008. Diagenesis and reservoir quality evolution of palaeocene deep-water, marine sandstones, the Shetland-Faroes Basin, British continental shelf. Marine Pet. Geol. 25, 514–543.
Morad, S., Ketzer, J.M., Deros, L.F., 2000. Spatial and temporal distribution of diagenetic alterations in siliciclastic rocks: implications for mass transfer in sedimentary basin. Sedimentology 47, 95–120.
Mullis, A.M., 1992. A numerical model for porosity modification at a sandstone-mudstone boundary by quartz pressure dissolution and diffusive mass transfer. Sedimentology 39, 99–107.
Peltonen, C., Marcussen, Ø., Bjørlykke, K., Jahren, J., 2009. Clay mineral diagenesis and quartz cementation in mudstones: the effects of smectite to illite reaction on rock properties. Marine Pet. Geol. 26, 887–898.
Qiu, N.S., Li, S.P., Zeng, J.H., 2004. Thermal history and tectonic-thermal evolution of the Jiyang Depression in the Bohai Bay Basin, East China. Acta. Geol. Sin. 78, 263–269, (In Chinese with English Abstract).
Rahman, M.J., McCann, T., 2012. Diagenetic history of the Surma Group sandstones (Miocene) in the Surma Basin, Bangladesh. J. Asian Earth Sci. 45, 65–78.
Ren, J., Zhang, L., Ezekiel, J., Ren, S., Meng, S., 2014. Reservoir characteristics and productivity analysis of tight sand gas in Upper Paleoz oic Ordos Basin China. J. Nat. Gas Sci. Eng. 19, 244–250.
Schmidt, V., Mcdonald, D.A., 1979. The role of secondary porosity in the course of sandstone diagenesis. SEPM Spec. Publ. 26, 175–207.
Song, G.Q., Jiang, Y.L., Liu, H., Cai, D.M., 2009. Pooling history of cracked gas in middle-deep reservoirs in Lijin-Minfeng areas of the Dongying sag. Nat. Gas Ind. 29, 14–17, (In Chinese with English Abstract).
Song, M.S., Li, C.L., Zhang, J.L., 2012. Fine division and correlation of conglomerate sedimentary cycles in Yanjia area of Dongying depression. Acta Pet. Sin. 33, 781–788, (in Chinese with English abstract).
Stoessell, R.K., 1987. Mass transport in sandstones around dissolving plagioclase grains. Geology 15, 295–298.
Surdam, R.C., Crossly, L.J., Hagen, E.S., Heasler, H.P., 1989. Organic-inorganic interactions and sandstone diagenesis. AAPG Bull. 73, 1–23.
Thyne, G., 2001. A model for diagenetic mass transfer between adjacent sandstone and shale. Marine and Petroleum Geology 18, 743–755.
Wan, N., Wang, Y., Cao, Y., Song, G., 2010. Overpressured fluid compartment and hydrocarbon accumulation of deep layer of Es4 in the north zone of Minfeng Sag, Dongying Depression. Acta Sedmentol. Sin. 28, 395–400, (In Chinese with English Abstract).
Wang, Y., Cao, Y., Ma, B., Liu, H., Gao, Y., Chen, L., 2014. Mechanism of diagenetic trap formation in nearshore subaqueous fans on steep rift lacustrine basin slopes-A case study from the Shahejie Formation on the north slope of the Minfeng Subsag, Bohai Basin, China. Petroleum. Sciences 11, 481–494.
Worden, R.H., Morad, S., 2000. Quartz cementation in oil field sandstones: a review of the key controversies. Spec. Publi. Int. Assoc. Sedimentol. 29, 1–20.
Xu, L., Cao, Y., Wang, Y., Huang, L., 2008. Genetic model of salt-gypsum rock of Paleogene in Dongying depression and its relationship with hydrocarbon reservoir. J. China Univ. Pet. 32, 30–35, (in Chinese with English abstract).
Zhu, G.Y., Gu, L.J., Su, J., Dai, J.X., Ding, W.L., Zhang, J.C., Song, L.C., 2012. Sedimentary association of alternated mudstones and tight sandstones in China's oil and gas bearing basins and its natural gas accumulation. J. Asian Earth Sci. 50, 88–104.
Zou, C.N., Zhu, R.K., Liu, K.Y., Su, L., Bai, B., Zhang, X.X., Yuan, X.J., Wang, J.H., 2012. Tight gas sandstone reservoirs in China: characteristics and recognition criteria. J. Pet. Sci. Eng. 88, 82–91.